


RESEARCH ARTICLE | SEPTEMBER 22 2020

# Development of a broad band AC power amplifier for real time turbulence feedback control experiment in the Saskatchewan Torus-modified (STOR-M) tokamak

Debjyoti Basu ; Masaru Nakajima; A. V. Melnikov; ... et. al



Rev Sci Instrum 91, 094707 (2020)

<https://doi.org/10.1063/5.0012014>



View  
Online



Export  
Citation

CrossMark

## Articles You May Be Interested In

Measurement of plasma rotation velocities with electrode biasing in the Saskatchewan Torus-Modified (STOR-M) tokamak

*Physics of Plasmas* (July 1994)

Control of the floating potential fluctuations via limiter biasing in the Saskatchewan Torus-Modified (STOR-M) tokamak

*Physics of Plasmas* (November 1994)

Retarding field energy analyzer for the Saskatchewan Torus-Modified plasma boundary

*Rev Sci Instrum* (October 2009)



Time to get excited.  
Lock-in Amplifiers – from DC to 8.5 GHz

[Find out more](#)

 Zurich  
Instruments

# Development of a broad band AC power amplifier for real time turbulence feedback control experiment in the Saskatchewan Torus-modified (STOR-M) tokamak

Cite as: Rev. Sci. Instrum. 91, 094707 (2020); doi: 10.1063/5.0012014

Submitted: 29 April 2020 • Accepted: 8 September 2020 •

Published Online: 22 September 2020



View Online



Export Citation



CrossMark

Debjyoti Basu,<sup>1,a)</sup> Masaru Nakajima,<sup>1</sup> A. V. Melnikov,<sup>2,3</sup> David McColl,<sup>1</sup> Chijin Xiao,<sup>1</sup> and Akira Hirose<sup>1</sup>

## AFFILIATIONS

<sup>1</sup>Plasma Physics Laboratory, University of Saskatchewan, Saskatoon S7N 5E2 Saskatchewan, Canada

<sup>2</sup>NRC Kurchatov Institute, 123182 Moscow, Russia

<sup>3</sup>National Research Nuclear University MEPhI, 115409 Moscow, Russia

<sup>a)</sup>Author to whom correspondence should be addressed: [debjyotibasubasu@gmail.com](mailto:debjyotibasubasu@gmail.com). Present address: Institute for Plasma Research, Bhat, Gandhinagar 382428, India.

## ABSTRACT

A gated oscillating power amplifier has been developed for high frequency biasing and real time turbulent feedback experiments in the Saskatchewan Torus-modified tokamak. This oscillator is capable of providing a peak to peak oscillating output voltage of around  $\pm 60$  V with a current around 30 A within the frequency band 1 kHz–50 kHz without any distortions. The overall output power is amplified by a two-stage metal oxide semiconductor field-effect transistor power op-amp as well as nine identical push-pull amplifiers in the final stages. The power amplifier input signal, collected from the plasma floating potential during the tokamak discharge, is optically isolated from the tokamak vessel ground. The filtered floating potential fluctuations with a band width of 5 kHz–40 kHz were amplified and fed to an electrode inserted into the plasma edge to study the response of the plasma turbulence. We observe that magnetic fluctuations are suppressed due to real time feedback of the floating potential.

Published under license by AIP Publishing. <https://doi.org/10.1063/5.0012014>

## I. INTRODUCTION

Tokamak configuration is considered a leading candidate for fusion energy power plants. The study of the process of transition from low confinement (particle and energy) mode to higher confinement (particle and energy) mode is one of the main aspects to build a fusion reactor where lower to higher confinement mode transition depends solely on the suppression of anomalous transport. The necessary condition to achieve burning plasmas in a fusion reactor is to control anomalous energy and particle transport where the turbulence is a key factor<sup>1</sup> for these anomalies. Real time feedback of turbulence at the edge plasma in tokamaks is a promising method to control electrostatic or electromagnetic turbulence. Earlier experiments showed that it is possible to feedback control and stabilize

plasma fluctuations or instabilities. The stabilization examples include ion-cyclotron mode in a mirror machine<sup>2</sup> and drift instabilities in linear machines.<sup>3,4</sup> Furthermore, stabilization of MHD modes was tried for the first time through a feedback technique in the adiabatic toroidal compressor machine.<sup>5</sup> In all these experiments, the feedback method dealt with a single mode or a small numbers of well defined modes in the frequency domain ( $\delta\omega \ll \omega$ ). Here, “ $\omega$ ” and “ $\delta\omega$ ” are the mode frequency and the frequency width of the mode.

Turbulence is more complex in tokamaks compared to linear or mirror machines. In tokamaks, strong nonlinear coupling between different modes results in broad band spectra with small wavelengths and small spatial correlation length in directions perpendicular to the toroidal magnetic field.<sup>6,7</sup> Real time feedback

control for electrostatic turbulence suppression has been tested in a few tokamaks such as TEXT,<sup>8</sup> KT-5C,<sup>9</sup> and more recently in the HBT-EP tokamak<sup>10</sup> to stabilize MHD mode rotation. All those simulation experiments using a biased electrode have revealed that real time feedback of electrostatic or magnetic modes may be a powerful means for active control of turbulence in reactor like devices, on the condition that the proper technology can be developed. In order to gain a clearer physical understanding, real time feedback experiments were performed in the Saskatchewan Torus-modified (STOR-M) tokamak. It is clear from previous experiments in the TEXT tokamak<sup>8</sup> that the success of active feedback control depends upon the following two basic parameters: (a) the gain of the feedback system and (b) the phase shift between the output and input turbulence signals over the frequency band. This article describes a simple electrostatic turbulence feedback control system developed to perform real time experiments with active feedback control on the STOR-M tokamak. This system mainly consists of a broadband power amplifier (1 kHz–50 kHz), optical isolator, and filter. The input of the feedback control system is the floating potential measured by a Langmuir probe, and the amplified signal is applied, either in phase or antiphase, to an electrode. Both the probe and the electrode are placed on the same magnetic surface in the edge plasma region. The main challenging task was to develop a broadband power amplifier, which can transfer wide band turbulent spectra without any distortion from its input to output.

In this article, elaborate descriptions of the experimental setup, power amplifier development, and its performance, experimental outcomes, and related physical explanations will be presented.

## II. EXPERIMENTAL SET UP

STOR-M is a small limiter tokamak with circular plasma cross section and major and minor radii  $R_0 = 46$  cm and  $a = 12$  cm, respectively. During real time feedback control experiments, the floating potential signal, collected from a Langmuir probe within an electronically gated time window, was amplified and fed into the plasma

through a rectangular electrode, made of a stainless steel plate. In this experiment, both the electrode and Langmuir probe were inserted from the horizontal ports at the low field side in the equatorial plane and placed on the same magnetic surface ( $r/a = 0.88$ ) although the ports are toroidally separated by  $180^\circ$ . The main plasma diagnostic systems included two additional floating potential probes inserted from the top and bottom port and a set of 12 Mirnov coils, which were separated toroidally by  $90^\circ$  in counter clockwise direction (top view) with respect to the location of the floating potential probes. A block diagram of an ideal active feedback system is shown in Fig. 1. The block diagram shows the various stages of the feedback process: collecting turbulent plasma spectra, processing the collected spectra, adjusting the phase shift between input and output signals, and applying the amplified output signal back to the plasma. The main components of the ideal feedback hardware consists of a Langmuir probe to measure the plasma floating potential, a voltage divider, optical isolator to avoid ground loops, analogue bandpass filter, phase shifter, power amplifier, and an electrode to apply the processed signal to the plasma. In our actual experiment, the processed feedback signal was supplied to the plasma using an electrode, either in phase or antiphase with respect to the measured turbulence waveform. The measured broadband turbulence floating potential signal is filtered in the frequency band 5 kHz–40 kHz, and an optical isolator is used to avoid ground loops. The power amplifier is the key component of the feedback system, and its block diagram is shown in Fig. 2. This power amplifier has been developed for either pre-programmed single mode high frequency biasing experiments<sup>11</sup> or real time broadband turbulence feedback control experiments. For operation in single-mode control, a function generator provides the input signal with a waveform with pre-selected amplitude and frequency. In a real feedback experiment, the input signal of the power amplifier is the filtered floating potential signal measured *in situ* with the Langmuir probe. The onset time of the input signal and its active time window during the plasma discharge was controlled through a master Transistor-Transistor Logic (TTL) pulse, which is generated by a pulse controller circuit. The STOR-M timing sequence

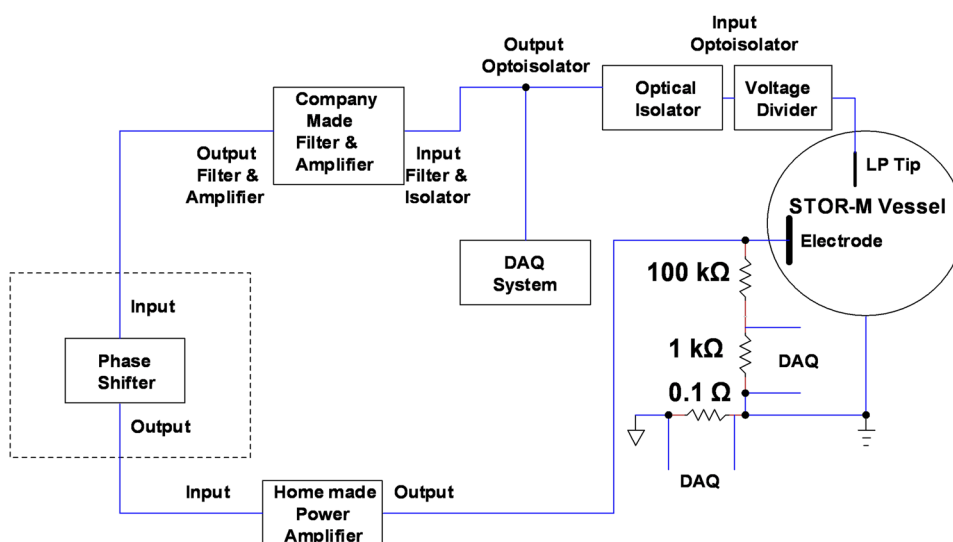


FIG. 1. Block diagram for an ideal active feedback system.

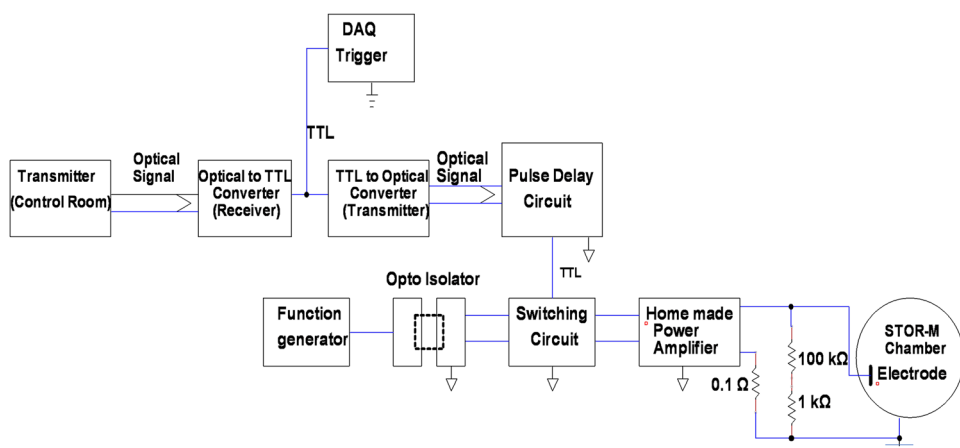


FIG. 2. Block diagram of the broadband power amplifier.

generator sends a fiber optical signal to the pulse controller circuit, which, in turn, generates a delayed rectangular TTL pulse with a pre-selected duration. This rectangular TTL pulse activates an analog solid-state switch LF13202 such that the floating potential signal is actually sent to the input of the power amplifier. Figure 3 shows the pulse delay control circuit, the optical isolator circuit, and the analog switch circuit. These three circuits were developed to modify conventional/recommended circuits according to the experimental needs. The key part of the pulse controller consists of an HFBR-25X1ETZ receiver, two NE555 timer units, and two 2N3904 NPN transistors. The HFBR-25X1ETZ receiver output is kept in the

high state when there is no optical signal. When the input photodiode receives the optical trigger, its output goes to the low state. Normally, the inputs of both NE555 timer units are kept at the high state and their outputs stay at the low state since both are configured for monostable operation. The first timer input is connected to the output of an optical receiver, and its output is connected to the base of both transistors in this circuit. The second timer input is connected to the collector of the first transistor such that it remains in the high state. Both timers are triggered at when the input signal jumps from the high to the low state and the output pulse width is controlled by a resistor and capacitor connected in series with a pulse

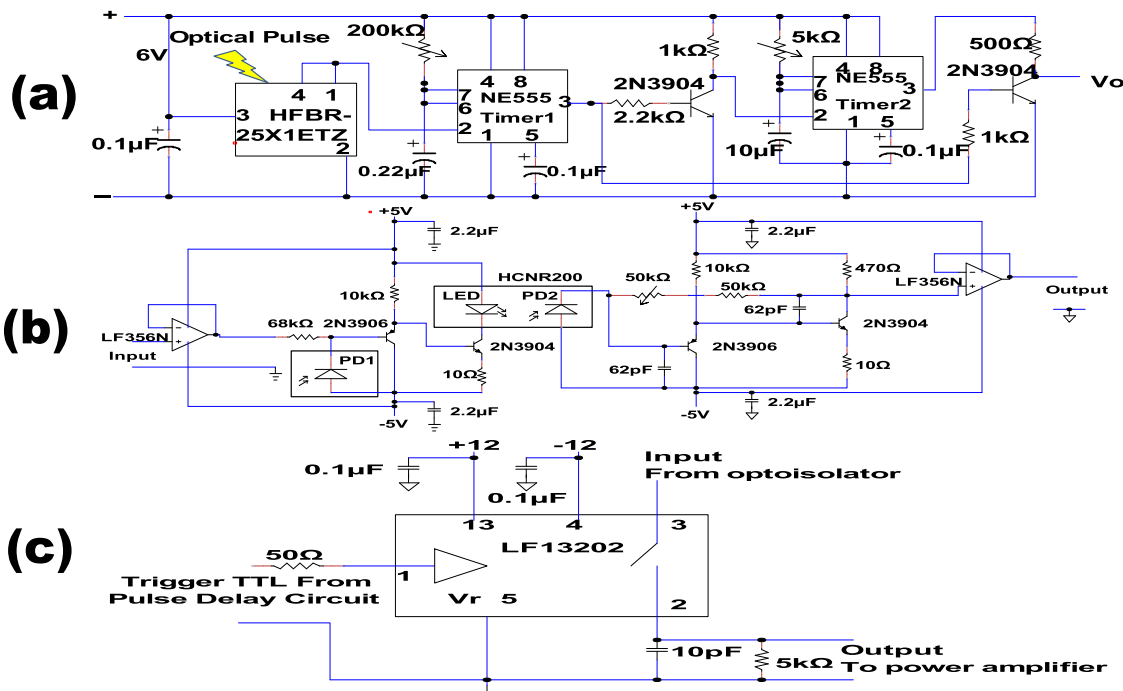


FIG. 3. Electronic circuit diagram of (a) pulse controller, (b) opto-isolator, and (c) solid-state electronic switch.

width given by  $t_w = 1.1RC$ . Finally, the output pulse of the pulse controller circuit is extracted from the collector of the second transistor. This jumps to the low state when the output of both timers is in the high state. It jumps to the high state when the base of the second transistor goes to the low state (from the first timer output) but its collector remains in the high state (from the second timer output), which then effectively turns off the transistor. It means that the output of the transistor jumps from the low state to the high state when the first timer's output jumps from the high to the low state and the second timer's output remains in the high state. As a result, the output pulse width of the pulse controller is determined by the subtracted value of the second and first timer output pulse width. The overall pulse delay time and pulse width can be varied between 0.5 ms and 44 ms and between 1 ms and 49 ms, respectively. It controls the active time window for the solid-state switch LF13202.

Figure 3(b) shows the optoisolator circuit needed to avoid ground loops. It uses a highly linear, high speed analog optocoupler HCNR200 with bandwidth from DC to 1.5 MHz as well as a maximum working insulation voltage  $V_{rms} = 1$  kV. The optoisolator circuit is made on the principle of auto current feedback using the HCNR200 where LED lights controls the photocurrent of the input and output photodiodes, which were used in reverse biased mode in their linear operation domain. The circuit recommended by the manufacturer has been modified and converted into a bipolar configuration. Two op-amp based voltage followers have been used to avoid signal distortion due to impedance mismatch at its input and output. The specifications of all components have been chosen and used in the circuit according to our requirements. Figure 3(c) shows the analog switching circuit where the electronic switch activation time is controlled by the output pulse of the pulse controller circuit. The input of the switch is connected with the output of the opto-isolator, and its output is connected to the input of power amplifier. The opto-isolator input signal consists in the floating potential during active feedback experiments or is provided by a function generator for single-mode operation in high frequency biasing experiments. The power amplifier amplifies the signal and sends it to an electrode located in the edge of STOR-M.

### III. POWER AMPLIFIER

A broadband power amplifier has been developed for the turbulence control experiments on STOR-M. It amplifies oscillating signals within the frequency range 1 kHz–50 kHz. The input signal with an oscillating voltage  $\pm 0.4$  V and a current  $\pm 0.5$  A is amplified to produce an output oscillating signal with a voltage around  $\pm 60$  V and current around  $\pm 30$  A without any distortion. The frequency band 1 kHz–50 kHz is chosen because the frequency of the density gradient driven drift mode calculated using the edge density gradient and edge temperature in STOR-M is around 10 kHz,<sup>12</sup> and the measured MHD mode has a frequency of about 20 kHz.<sup>13</sup> The power amplifier unit has two consecutive sections that amplify separately the voltage and the current. The speed, bandwidth, and the slew rate of all integrated circuits (ICs) used in the electronic design have been carefully selected to optimize the specifications for the bandwidth and the phase properties of the power amplifier. The voltage and current amplification sections are discussed in detail in Secs. III A and III B.

### A. Voltage amplification unit

The voltage amplification unit receives signal through a capacitor to remove a possible DC offset. It has an op-amp based voltage follower and two op-amp based voltage amplifiers. Each section of this unit is connected to the next one through a capacitor to avoid DC offsets arising from a possible DC biasing of each op-amp. This is shown in Fig. 4.<sup>11</sup> The voltage follower of this unit has been designed using an LF356N op-amp for impedance matching with the circuit that follows. The input voltage is amplified using a high speed power MOSFET op-amp PA340CC having a large frequency bandwidth and high frequency response. It has a peak to peak biased voltage and peak current rating of 350 V and 120 mA, respectively, but the peak to peak biased voltage and continuous current rating for a safe operating range are 250 V and 60 mA, respectively. Its differential input voltage can be varied from  $-16$  V to  $+16$  V. The Gain Bandwidth Product (GBWP at 1 MHz), slew rate (at a compensation capacitance of 4.7 pF), and power bandwidth (PB) (at peak to peak voltage 280 V) are 10 MHz, 32 V/ $\mu$ s, and 35 kHz, respectively. The amplification is accomplished using two inverting op-amp amplifiers where the amplification factor of the first stage and second stage are 17.5 and 10, respectively. As a result, the equivalent amplification factor is around 175. The output current of the voltage amplifier is limited by a 330  $\Omega$  resistance, connected to the second stage of the op-amp. With a biasing voltage of  $\pm 120$  V and a maximum current of 38 mA, its power dissipation is 9 W, which is well below the continuous safe operating power dissipation of 14 W.

To understand the frequency response of this circuit, we need to calculate the GBWP (Gain Band Width Product) and power bandwidth. For an op-amp, the GBWP is defined by  $GBWP = GAIN \times f_{BW}$ , where  $f_{BW}$  is the frequency bandwidth. GBWP is a constant over a wide range of frequencies for an op-amp even beyond its cutoff frequency. For the amplifier we used, PA340CC, a GBWP = 10 MHz translates into a GAIN = 10 when  $f_{BW} = 1$  MHz. For the first stage of the inverting amplification with a GAIN = 17.5, we find  $f_{BW} = 570$  kHz since GBWP = 10 MHz. This means that the voltage amplifier can amplify signals with frequency up to 570 kHz. However, this does not tell us whether the output signal will be distorted or not. To determine the frequency range for an undistorted signal in the output of the voltage amplifier, we need to calculate the power bandwidth (PB) given by  $PB = \frac{SlewRate}{2\pi V_p}$ . Here,  $V_p$  is the peak output voltage of the oscillatory signal. Thus, we find for PB = 72 kHz with a slew rate = 32 V/ $\mu$ s and  $V_p = 70$  V. Therefore, the designed voltage amplifier is able to generate an undistorted output signal up to 70 kHz with a peak oscillating voltage of 70 V.

### B. Current amplification unit

A push-pull amplifier (class "AB") has been used for the power amplification section, which is shown in Fig. 5.<sup>11</sup> Complementary Darlingtons silicon power transistors MJH11021(PNP) and MJH11022(NPN) have been used for the power amplification. MJH11021 and MJH11022 have been chosen because these two ICs have a maximum sustainable voltage collector-emitter ( $V_{CE}$ ) = 250 Vdc, collector-base ( $V_{CB}$ ) = 250 Vdc and emitter-base ( $V_{EB}$ ) = 5 Vdc as well as maximum collector current ( $I_C$ ) = 10 Adc, base current ( $I_B$ ) = 0.5 Adc, power rating ( $P_D$ ) = 150 W, dc current gain ( $h_{fe}$ )  $h_{femin} = 400$  and  $h_{femax} = 15000$ , and current-gain bandwidth

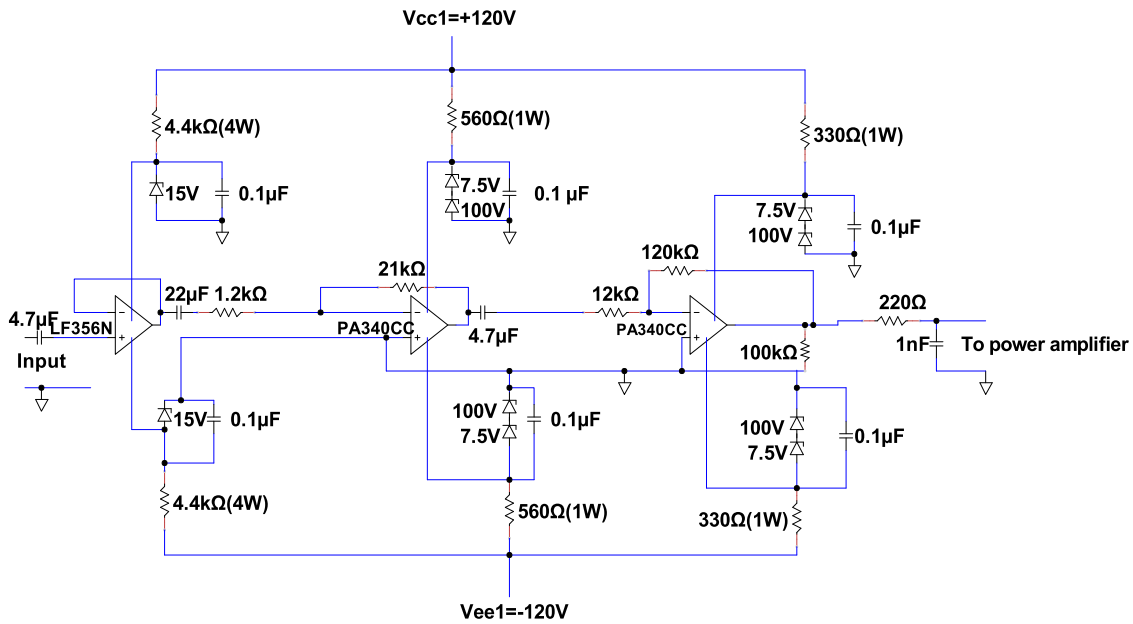


FIG. 4. Voltage amplification unit of the power amplifier.

product ( $f_T$ )  $f_{Tmin} = 3$  MHz at ( $I_C = 10$  Adc,  $V_{CE} = 3$  Vdc, and  $f = 1$  MHz). Nine identical push-pull amplifiers connected in parallel have been used at the final stage for current amplification. The designed circuit controls, the base current  $I_B$  of these nine identical amplifiers, and the maximum value of  $I_B$  were kept within 70 mA. We also used a buffer stage between the voltage amplifier and the

final current amplification stage to provide a sufficiently large base current. Since the final output is applied to the plasma through an electrode, the power amplifier should obviously be capable to deliver a large amount of electron current in the positive half of the oscillatory signal. Here, a maximum rated current of 30 A is designed when the DC biased voltage of each push-pull amplifier section

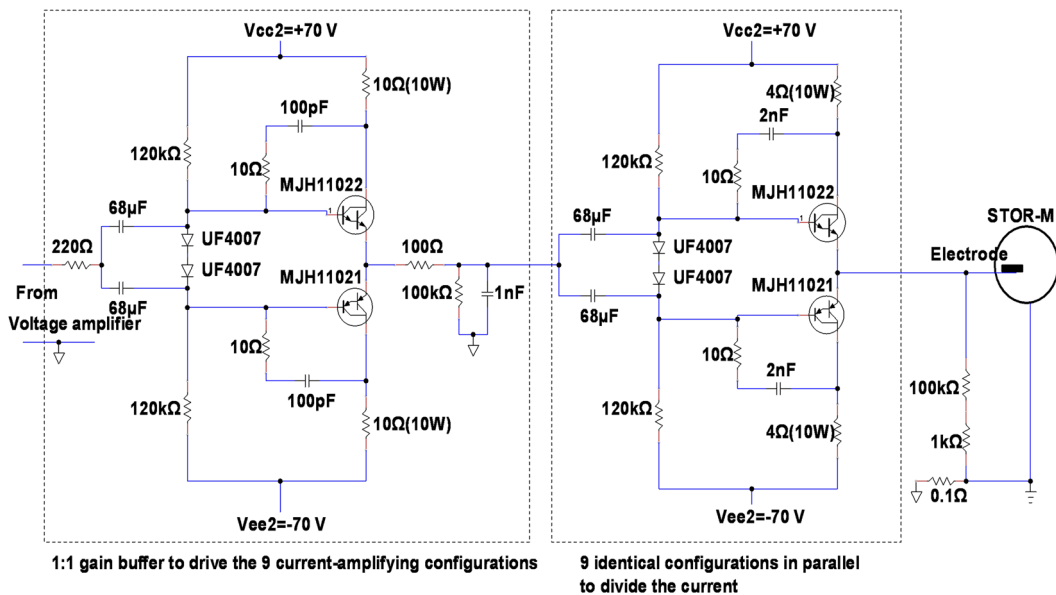
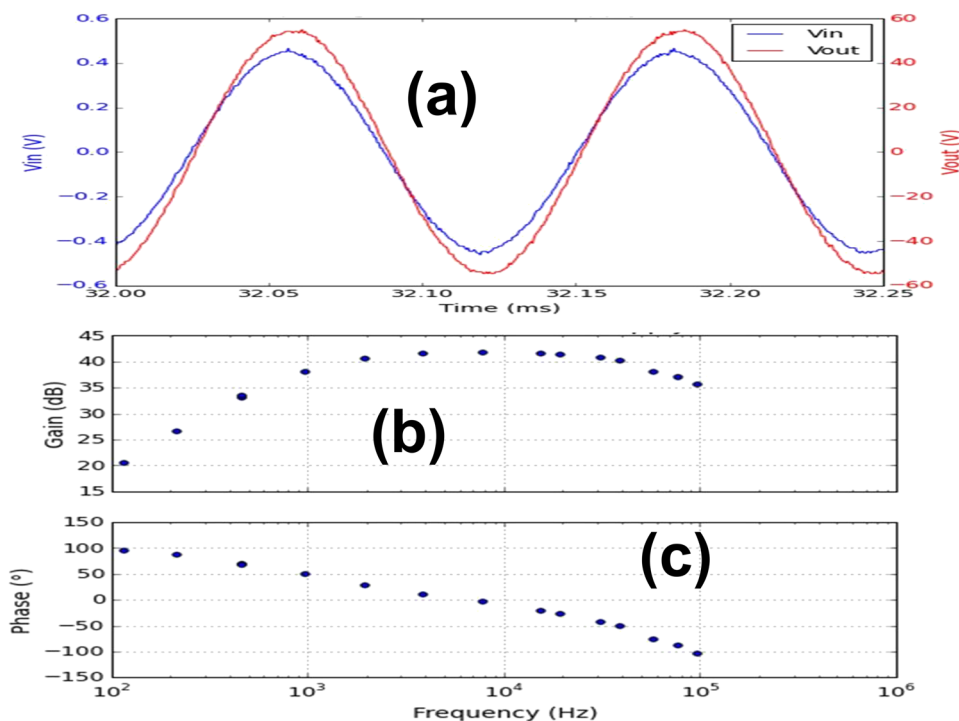


FIG. 5. Current amplification unit of the power amplifier.



**FIG. 6.** Typical example of (a) input and output signal with time, (b) frequency vs gain, and (c) frequency vs the phase difference between the input and the output signal of the power amplifier.

is  $\pm 70$  V. The typical circuit performance is shown in Fig. 6. Figure 6(a) shows typical waveforms for the input and output voltage signals. This shows that the output signal peak value is 56 V. According to the IC characteristics for  $V_{CE} = 1$  V, the calculated value for the current is 3.25 A since the supply voltage is  $\pm 70$  V with a current limiting resistance of  $4 \Omega$  (10 W). Therefore, the total current rated for the power amplifier is  $\sim 30$  A. A successful bench test of the power amplifier in pulsed mode was performed using a minimum load resistance of  $2 \Omega$  (2000 W) with no noticeable distortion of the output signal. If a larger current is required for this circuit, then the biasing voltage of this section needs to increase to more than  $\pm 70$  V. The crossover distortion at zero voltage was overcome by two identical diodes UF4007 with two identical biasing capacitors of  $68 \mu\text{F}$ . It should be pointed out that the current gain, as follows from the characteristics, is around  $h_{fe} = 1500$ . Figure 6(b) shows the overall frequency response of the power amplifier demonstrating that its power gain (A) is around 43 dB within the frequency range 1 kHz–50 kHz. The power gain in the diagram is defined by gain (A)  $= 10 \log(P_{out}/P_{in}) \approx 20 \log(V_{out}/V_{in})$ , where the input resistance ( $R_{in}$ )  $\approx$  output resistance ( $R_{out}$ ) [ $(R_{out}/R_{in}) = 2.5$ ]. Figure 6(c) shows that the phase variation between the input and the output obtained during a performance test lies between  $\pm 50^\circ$  for the frequency range 1 kHz–50 kHz.

#### IV. RESULTS AND DISCUSSION

The power amplifier was successfully used for a high frequency biasing experiment<sup>11</sup> or single frequency operation mode on STOR-M, and improved confinement was successfully achieved. In real

time feedback experiments, the signal of the floating potential within a selected time window has been fed to the biasing electrode. The flowchart shown in Fig. 1 indicates that the floating potential signal from the Langmuir probe is transferred through an optical isolator to avoid ground loops and then filtered through a bandpass filter with a bandwidth between 5 kHz and 40 kHz. Ideally, this filtered frequency should be sent through a broad band phase shifter, but in our case, it is directly connected to the input of the power amplifier. Figure 7 shows an example of the waveforms of the plasma parameters during a typical STOR-M discharge with real time feedback of the floating potential applied to the plasma through the electrode during the selected time window 13 ms–20 ms. The  $H_\alpha$  emission intensity level did not change significantly during the active turbulence feedback time window as compared of the signal level before and after feedback.

The floating potential signal and the voltage applied to the electrode by the power amplifier are highly coherent within the targeted frequency range 5 kHz–40 kHz, as shown in Fig. 8(a). However, the phase shift between the two signal changes from  $0^\circ$  to  $-90^\circ$ , within the same frequency range as shown in Fig. 8(b).

Initially, it is observed whether any abrupt perturbation arises or not during application of active feedback such that plasma condition may be deteriorated. Both floating potential and Mirnov fluctuations have been studied. Comparison is made for fluctuations during the time windows: before (10 ms–13 ms), within (13 ms–16 ms and 17 ms–20 ms), and after feedback (20 ms–23 ms). Note that the floating potential fluctuation level within the feedback time window is not changed compared with those before and after feedback, as shown in Fig. 9.

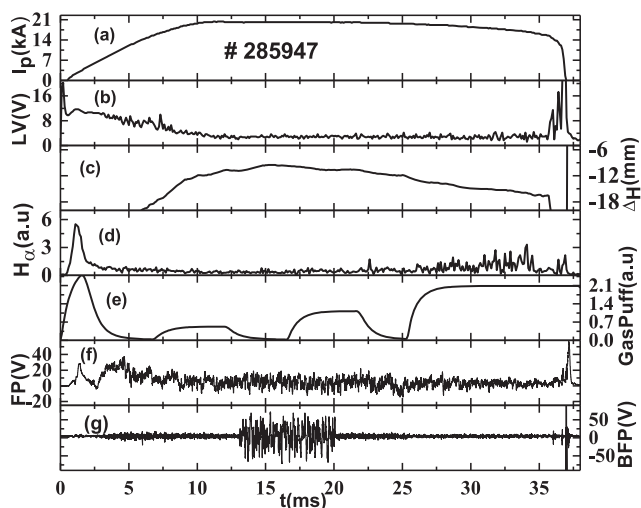


**FIG. 7.** Temporal evolution of (a) plasma current, (b) loop voltage, (c) plasma horizontal position, (d) plasma  $H_\alpha$  intensity, (e) gas puff, (f) floating potential, and (g) feedback of the floating signal.

This clearly indicates that the PSD (Power Spectral Density) within the 3 ms time window of top and bottom floating potential fluctuations before (red solid line) and after (blue solid line) feedback did not change significantly comparing with the PSD during the application of the feedback system (black dotted lines) of the same signal. However, interestingly, it is noticed that magnetic fluctuation suppression occurs within the feedback time window as compared to before or after the feedback everywhere in the plasma poloidal cross section. Figure 10 shows PSDs of Mirnov signals measured by probes located at four poloidal locations corresponding to (a) outboard, (b) top, (c) inboard, and (d) bottom. The magnetic fluctuations were clearly suppressed during the feedback (red solid line) as compared to those before the feedback (black solid line).

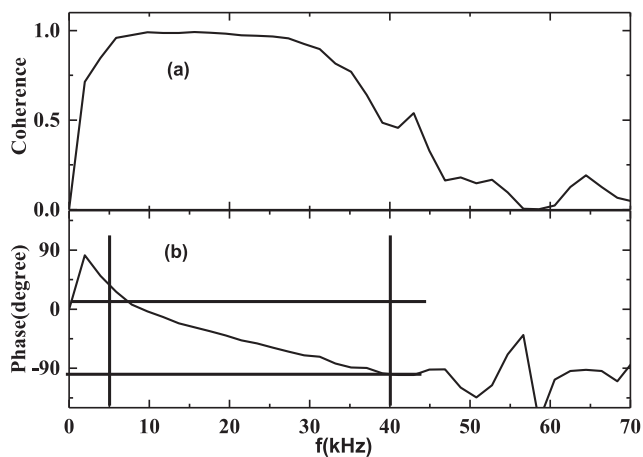


**FIG. 8.** Frequency dependence of (a) cross-coherence and (b) phase difference between the floating potential and the feedback signal.

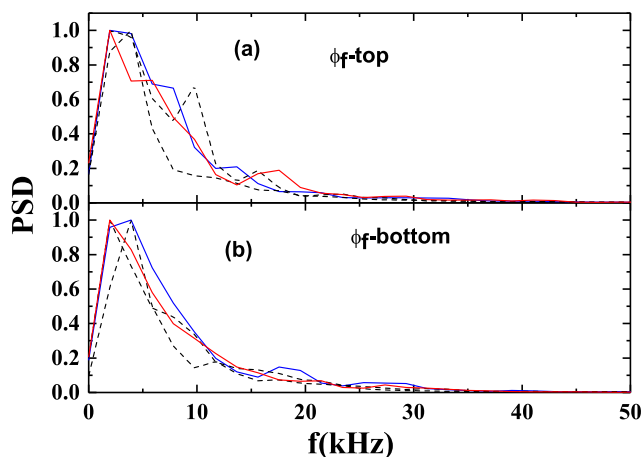


**FIG. 9.** Frequency dependence of the PSD measured by (a) top and (b) bottom floating potential signals before (red solid line, 10 ms–13 ms), during (two black dotted lines, 13 ms–16 ms and 17 ms–20 ms), and after (blue solid line, 20 ms–23 ms) the application of the feedback system.

The array of 12 Mirnov probes evenly distributed at 12 poloidal angles can be used to infer the poloidal mode of the magnetic fluctuations.

Spatial poloidal mode structures of Mirnov oscillations have been derived using a Singular Value Decomposition (SVD) code<sup>14</sup> within three time windows: before feedback (10 ms–13 ms) and during feedback (13 ms–16 ms and 17 ms–20 ms). It shows that a spatial mode structure ( $m = 4$ ) has been stabilized. Its structure remains unchanged, and it does not continue to grow. Mode structure evolution is shown in Fig. 11 before (black line, 10 ms–13 ms) and during the feedback phase [(red line) 13 ms–16 ms and (blue line) 17 ms–20 ms].

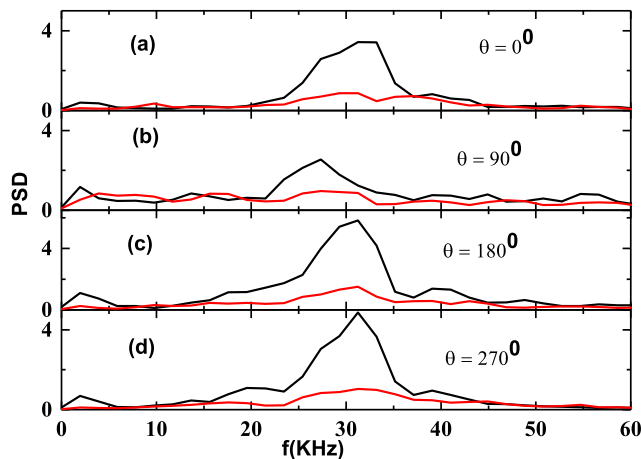


**FIG. 10.** Frequency dependence of the PSD measured by (a) radially outboard, (b) top, (c) radially inboard, and (d) bottom Mirnov signals before (black solid line, 10 ms–13 ms) and during (red solid line, 13 ms–16 ms) the application of the feedback system.



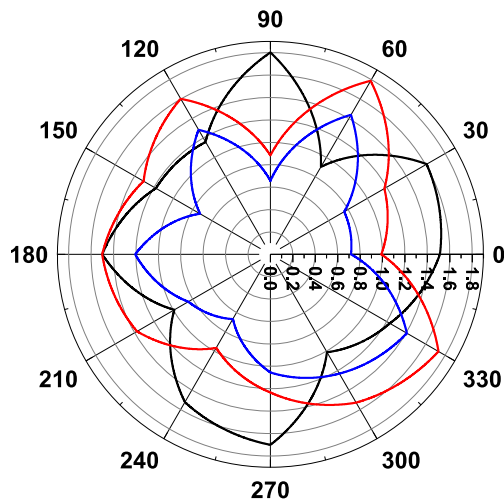


**FIG. 11.** Evolution of the spatial mode structure before (black solid line, 10 ms–13 ms) and during (red solid line, 13 ms–16 ms and blue solid line, 17 ms–20 ms) feedback.

## V. CONCLUSIONS

A successful active feedback of turbulence has been performed in the STOR-M tokamak with free phase drifting of the floating potential fluctuations. Interestingly, we found that the plasma electrostatic turbulence is not enhanced and that the magnetic fluctuations have been suppressed during the feedback control. This experiment indicates that active electrostatic turbulent feedback may be another possible means by which MHD fluctuations and modes may be stabilized. In the future, a phase shifter may be used to actively adjust the phase for the desired frequency ranges and to study its effects on the plasma turbulence in the STOR-M tokamak. The quantitative investigation of the effects of the feedback output voltage polarity and gains on the turbulence modes were not investigated in the present experimental studies, which remains an important future work.

## ACKNOWLEDGMENTS

The authors would like to acknowledge NSERC for supporting this work. They would also like to acknowledge the support provided

by our machine workshop. Special acknowledgment and gratitude go to Mr. Chomyshen and Mr. Toporowski in the machine workshop for their kind help and friendly approach when needed. They would like to appreciate Professor Jef Ongena for his careful reading of this manuscript, valuable comments and text improvements. The work of Professor A.V.M. was supported by the Russian Science Foundation (Project No. 19-12-00312) and, in part, by the Competitiveness Programme of the National Research Nuclear University “MEPhI.”

## DATA AVAILABILITY

The data that support the findings of this study are available from the corresponding author upon reasonable request.

## REFERENCES

- R. V. Bravenec, D. W. Ross, P. M. Schoch, D. L. Brower, J. W. Heard, R. L. Hickok, P. W. Terry, A. J. Wootton, and X. Yang, *Nucl. Fusion* **31**, 687 (1991).
- V. V. Arsenin, V. A. Zhil'tsov, V. Kh. Likhstenshtein, and V. A. Chulnov, *JETP Lett.* **8**, 41 (1968); ; available at [http://www.jetpletters.ac.ru/ps/1704/article\\_25911.shtml](http://www.jetpletters.ac.ru/ps/1704/article_25911.shtml)
- R. R. Parker and K. I. Thomassen, *Phys. Rev. Lett.* **22**, 1171 (1969).
- B. E. Keen and R. V. Aldridge, *Phys. Rev. Lett.* **22**, 1358 (1969).
- K. Bol, J. L. Cecchi, C. C. Daughney, F. DeMarco, R. A. Ellis, Jr., H. P. Eubank, H. P. Furth, H. Hsuan, E. Mazzucato, and R. R. Smith, in *Proceedings of the Fifth International Conference on Plasma Physics and Controlled Nuclear Fusion Research* (International Atomic Energy Agency (IAEA), Tokyo, 1974), Vol. 1, p. 83.
- P. C. Liewer, *Nucl. Fusion* **25**, 543 (1985).
- J. D. Callen, *Phys. Fluids B* **4**, 2142 (1992).
- T. Uckan, B. Richards, R. D. Bengtson, B. A. Carreras, G. Li, P. D. Hurwitz, W. L. Rowan, H. Y. W. Tsui, and A. J. Wootton, *Nucl. Fusion* **35**, 487 (1995).
- Z. Kan, W. Yi-zhi, Y. Chang-xuan, L. Wan-dong, W. Chao, Z. Ge, and X. Zhi-zhan, *Phys. Rev. E* **55**, 3431 (1997).
- J. W. Brooks, I. G. Stewart, M. D. Boyer, J. P. Levesque, M. E. Mauel, and G. A. Navratil, *Rev. Sci. Instrum.* **90**, 023503 (2019).
- D. Basu, M. Nakajima, A. V. Melnikov, J. J. Martinell, D. McColl, R. Singh, C. Xiao, and A. Hirose, *Nucl. Fusion* **60**, 094001 (2020).
- D. Basu, M. Nakajima, A. V. Melnikov, D. McColl, A. Rohollahi, S. Elgriw, C. Xiao, and A. Hirose, *Nucl. Fusion* **58**, 024001 (2018).
- C. Xiao, T. Niu, J. E. Morelli, C. Paz-Soldan, M. Dreval, S. Elgriw, A. Pant, D. Rohraff, D. Trembach, and A. Hirose, *Rev. Sci. Instrum.* **79**, 10E926 (2008).
- S. Elgriw, D. Liu, T. Asai, A. Hirose, and C. Xiao, *Nucl. Fusion* **51**, 113008 (2011).